Bioinorganic Chemistry

DOI: 10.1002/anie.200803418

A Synthetic Analogue of Rieske-Type [2Fe-2S] Clusters**

*Joachim Ballmann, Antonia Albers, Serhiy Demeshko, Sebastian Dechert, Eckhard Bill, Eberhard Bothe, Ulf Ryde, and Franc Meyer**

In 1964 Rieske type [2Fe-2S] clusters were discovered in biological systems and identified as variants of [2Fe-2S] ferredoxins.[1] Structurally they differ form the parent ferredoxins by an asymmetrical terminal ligation at the [2Fe-2S] core, with only one iron center coordinated by two cysteinyl thiolates and the other coordinated by two histidine nitrogen donors.[2] Spectroscopic (e.g. EPR and Mössbauer) and functional characteristics (namely the electrochemical potential) of Rieske type [2Fe-2S] clusters are distinct because of this unique coordination environment.[3] The investigation of synthetic model complexes has provided valuable insight into the properties and electronic structures of iron–sulfur cofactors.[4] While several biomimetic [2Fe-2S] clusters with all-S or all-N environments have been obtained over the last decades,[4,5] no asymmetrically ligated cluster that emulates the particular situation of the Rieske iron–sulfur proteins could be synthesized to date.[6] Herein we report the synthesis as well as spectroscopic and crystallographic characterization of the first accurate synthetic model compound **4** for Rieske type [2Fe-2S] clusters.

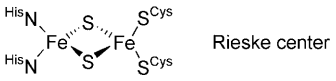

A stepwise ligand exchange strategy starting from $[NEt_4]_2[Fe_2S_2Cl_4]$[7] (**1**) was discovered to be a suitable synthetic approach affording the first asymmetrically coordinated [2Fe-2S] clusters. After extensive ligand screening, a backbone phenyl substituted chelating diskatylmethane[8] $\{N_2\}$ capping ligand, which serves as a mimic for the natural histidine residues, was found to suppress the usually preferred formation of the homoleptic N- and S-coordinate cluster compounds. Addition of the deprotonated $\{N_2\}$ ligand to a cooled solution of **1** led to the isolation of the partially substituted intermediate $[NEt_4]_2[\{N_2\}Fe_2S_2Cl_2]$ (**2**, Scheme 1).

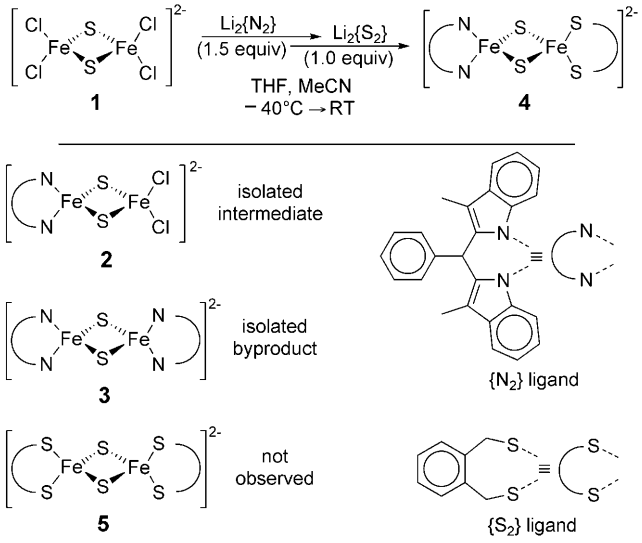

Scheme 1. Synthesis of the synthetic analogue **4**. Cluster compounds **1**–**4** were used or obtained as NEt_4^+ salts.

Minor amounts of the N-homoleptic cluster $[NEt_4]_2[\{N_2\}Fe_2S_2\{N_2\}]$ (**3**) were formed as a byproduct and identified by X-ray diffraction (Figure S38 in the Supporting Information). Compound **2** was crystallized for X-ray diffraction (Figure 1, top) by diffusion of diethyl ether into a DMF solution. Prominent intracore distances and angles, as well as bond lengths and angles to the terminal donor atoms, are in agreement with the corresponding values determined for the related homoleptic $\{N_4\}$- or $\{Cl_4\}$-ligated[7] synthetic [2Fe-2S] clusters **3** and **1** (Table 1 and Table S6 in the Supporting Information).

The Rieske type cluster **4** can be prepared from **2**, but it is most conveniently obtained in a one-pot synthesis at −40 °C by sequential addition of the lithium salt of the $\{N_2\}$ ligand to **1** and subsequent addition of the deprotonated $\{S_2\}$ ligand *o*-xylene-α,α′-dithiol[9] (Scheme 1). The latter serves as a mimic for the biological cysteinyl thiolates. In contrast to previously studied combinations of nitrogen- and sulfur-donor ligands, no equilibrium between **4** and the corresponding homoleptic

[*] Dipl.-Chem. J. Ballmann, A. Albers, Dr. S. Demeshko, Dr. S. Dechert, Prof. Dr. F. Meyer
Institut für Anorganische Chemie
Georg-August-Universität Göttingen
Tammannstrasse 4, 37077 Göttingen (Germany)
Fax: (+49) 551-39-3063
E-mail: franc.meyer@chemie.uni-goettingen.de
Homepage: http://www.meyer.chemie.uni-goettingen.de
Dr. E. Bill, Dr. E. Bothe
Max-Planck-Institut für Bioanorganische Chemie
Stiftstrasse 34–36, 45470 Mülheim an der Ruhr (Germany)
Prof. Dr. U. Ryde
Department of Theoretical Chemistry, Lund University
Chemical Centre, S-22100 Lund (Sweden)

[**] Financial support by the DFG (International Research Training Group GRK 1422 "Metal Sites in Biomolecules: Structures, Regulation and Mechanisms"; see www.biometals.eu) and the Fonds der Chemischen Industrie (Kekulé fellowship for J.B.) is gratefully acknowledged.

Supporting information for this article is available on the WWW under http://dx.doi.org/10.1002/anie.200803418.

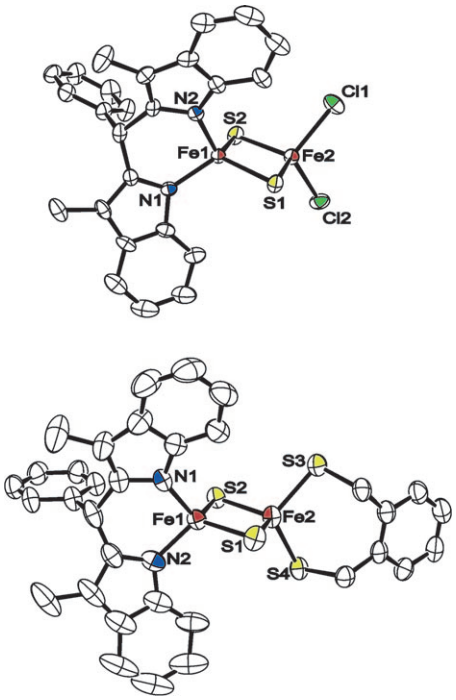

Figure 1. ORTEP plots (thermal ellipsoids set at 50% probability) of the molecular structures of **2** (top) and **4** (bottom). For clarity all hydrogen atoms and NEt_4^+ counterions are omitted.

Table 1: Selected interatomic distances (Å) for **1**–**5**.

Cmpd	d(Fe···Fe)	d(Fe–S)[a]	d(Fe–N)	d(Fe–Cl)
1[b]	2.716(1)	–	–	2.245(1) 2.258(1)
2	2.7124(9)	–	1.965(5) 1.975(4)	2.249(2) 2.273(2)
3	2.7562(8)	–	1.975(2) 1.984(3)	–
4	2.7027(8)	2.297(1) 2.291(1)	1.953(4) 1.975(4)	–
5[c]	2.698(1)	2.306(1) 2.303(1)	–	–

[a] Entry refers to the terminal sulfur atoms only. [b] Reference [7]. [c] Reference [9].

compounds **3** and **5** was detected. Isolated **4** is stable in the solid state at room temperature under an atmosphere of dry dinitrogen and can even be handled in air for short periods (ca. 30 min) without decomposition. In the absence of protic solvents, solutions of **4** can be stored for weeks at room temperature under an atmosphere of dry dinitrogen. Black plates suitable for X-ray diffraction (Figure 1, bottom) were obtained by slow diffusion of diethyl ether into a concentrated solution of **4** in DMSO. Geometric parameters at the two metal ions Fe1 and Fe2 are similar to the corresponding values for the homoleptic $\{N_4\}$- and $\{S_4\}$-ligated[9] compounds **3** and **5** (Table 1 and Table S6 in the Supporting Information). Compared to the Rieske proteins, only the Fe–N bond lengths and the N-Fe-N angles in **4** differ slightly—these differences most likely result from the protonated state of the histidine moieties in the proteins in contrast to the dianionic $\{N_2\}$ ligand in the model complex. Other geometric parameters agree well with those found for the natural systems (see Table S7 in the Supporting Information).[2c]

Two distinct quadrupole doublets are observed in the zero-field Mössbauer spectrum of **4** (Figure 2, Table 2), with

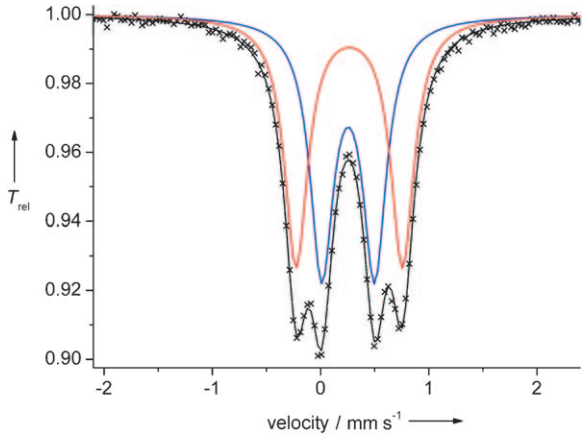

Figure 2. Zero-field Mössbauer spectrum of **4** recorded at 80 K. Isomer shifts and quadrupole splittings are summarized in Table 2; ∗: experimental data, ——/——: simulated subspectra (quadrupole doublets), ——: fit (sum of subspectra).

Table 2: Analytical data for clusters **2** and **4** together with the corresponding data for the related homoleptic compounds **1** and **5**.

Cmpd	δ (ΔE_Q)[a] [mm s^{-1}]	J[b] [cm^{-1}]	$E_{1/2}$[c] [V]
1[d]	0.37 (0.82)[e]	−158	−1.02[f]
2	0.32 (0.99); 0.32 (0.72)	−184	−1.25[g]
4	0.26 (0.49); 0.27 (0.98)	−161	−1.35
5[h]	0.28 (0.36)	−149 ± 8	−1.51[i]

[a] ^{57}Fe Mössbauer parameters at 80 K relative to iron metal at room temperature. [b] Values obtained from fits to SQUID data. [c] Potentials in DMF/0.1 M NBu_4PF_6 at a scan rate of 100 mV s^{-1} vs. the $[Cp^*_2Fe]/[Cp^*_2Fe]^+$ couple ($Cp^* = C_5Me_5$). [d] Reference [7]. [e] This work (Figure S27 in the Supporting Information). [f] Cathodic peak potential of the irreversible process recorded in MeCN/0.1 M NBu_4Cl vs. SCE is −1.00 V, corresponding to −1.02 V vs. $[Cp^*_2Fe]/[Cp^*_2Fe]^+$. [g] Cathodic peak potential of the irreversible process. [h] Reference [9]. [i] Half-wave potential $E_{1/2}$ in DMF vs. SCE is −1.49 V, corresponding to −1.51 V vs. $[Cp^*_2Fe]/[Cp^*_2Fe]^+$.

isomer shifts (0.26 and 0.27 mm s^{-1}) and quadrupole splittings (0.49 and 0.98 mm s^{-1}) that are in the same range as those observed for the natural Rieske proteins (see Table S2 in the Supporting Information). As intuitively expected, previously reported for the biological systems,[10] and apparent from comparison with **5**, the larger quadrupole doublet (red line in spectrum) reflects the N-coordinate Fe1 center and the smaller one (blue line) reflects the S-coordinate Fe2 center. Essentially the same considerations apply to cluster compound **2**, which is also ligated in an asymmetrical fashion (Table 2, Figure S28 in the Supporting Information).

Magnetic susceptibility measurements for **2** and **4** were carried out at a magnetic field $B = 0.5$ T from 295 to 2.0 K. Magnetic moments μ_{eff} were found in the range 2.3–0.8 μ_B, that is, much lower than expected for two uncoupled ferric

($S=5/2$) ions, and they rapidly decrease upon lowering the temperature (plots of μ_{eff} vs. T for **2** and **4** are shown in Figures S30 and S31, respectively, in the Supporting Information). This behavior is in accordance with strong antiferromagnetic coupling between the two ferric ions to give an $S=0$ ground state, as is usually observed for $[2Fe\text{-}2S]^{2+}$ clusters. Coupling constants J (Table 2) were determined by using a fitting procedure to the appropriate Heisenberg spin Hamiltonian for isotropic exchange coupling and Zeeman interaction: $H=-2J\vec{S}_1\vec{S}_2+g\mu_B(\vec{S}_1+\vec{S}_2)\vec{B}$. Interestingly, J values for the two asymmetrically coordinated compounds **2** and **4** indicate stronger antiferromagnetic coupling than in the related homoleptic clusters **1** and **3**.

All new clusters **2**–**4** show a series of partially overlapping electronic absorption bands (UV/Vis spectra depicted in Figures S4–S6 in the Supporting Information), but a more detailed analysis will be required to assign the different charge-transfer transitions. Reasonably well resolved ^{1}H NMR spectra could be recorded because of the strong antiferromagnetic coupling, and signal sets for the $\{N_2\}$ ligand and the $\{S_2\}$ ligand can be clearly distinguished (Figure S25 in the Supporting Information). Positive and negative ESI mass spectra for all cluster compounds show dominant signals for ions $[M+NEt_4]^+$ and $[M-NEt_4]^-$, respectively (Figures S8–S17 and S21–S23 in the Supporting Information).

Redox properties of **2** and **4** were studied by cyclic voltammetry in DMF/0.1 M NBu_4PF_6 at room temperature. The Rieske type cluster **4** exhibits a reversible one-electron reduction at −1.35 V versus decamethylferrocene and a second irreversible reduction wave at approximately −2.0 V, corresponding to formation of the all-ferrous species. Thus, the half-wave potential corresponding to the $[2Fe\text{-}2S]^+/[2Fe\text{-}2S]^{2+}$ pair of **4** is shifted slightly positive compared to the one-electron reduction wave observed for the homoleptic $\{S_4\}$-ligated analogue (−1.51 V).[9a] As expected, the unusually high redox potentials of the biological Rieske sites are not reflected by the model cluster **4**, owing to the dianionic character of the coordinated $\{N_2\}$ ligand instead of the protonated neutral histidine residues. Since this first-generation synthetic model cannot undergo the same protonation-assisted electron transfer as the natural counterpart, which relies on the peripheral histidine N atoms as protonation sites,[11] a dependence of the redox potential on the presence of proton sources is ruled out. Reduction of **2** is irreversible on the timescale of the cyclic voltammetry, as also observed for the homoleptic $\{Cl_4\}$-ligated cluster[7c] (Table 2, Figures S32 and S33 in the Supporting Information).

The one-electron-reduced mixed-valent species was generated from **4** in MeCN solution by constant potential coulometry (CPC) at −25 °C. Reduction was carried out at −1.9 V versus $[Cp_2Fe]/[Cp_2Fe]^+$ (−1.39 V vs. $[Cp^*_2Fe]/[Cp^*_2Fe]^+$). The progress was monitored by UV/Vis spectroscopy (Figure 3). Spectra were recorded every 1.5 min directly in the coulometric cell, and collection was stopped after a charge consumption of approximately 300 mC (calculated for one-electron reduction: 304 mC, see Figure S35 in the Supporting Information). Over the time of the coulometric experiment (ca. 13.5 min total), intensities of the main visible bands decreased; two isosbestic points were detected. Cyclic

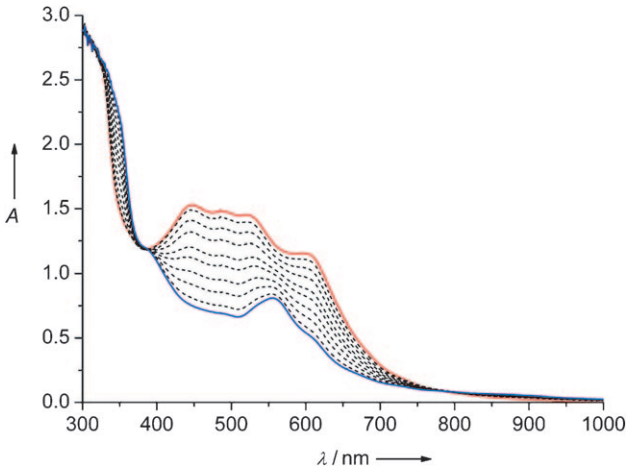

Figure 3. UV/Vis spectra recorded during constant-potential coulometry of **4** at −25 °C, −1.9 V vs. $[Cp_2Fe]/[Cp_2Fe]^+$, ——: $t_0=0$ min, ••••• and —— (after ca. 13.5 min): $t_0+n\Delta t$, $\Delta t=1.5$ min, $n=1$–9, $c=3.94\times10^{-4}$ M in MeCN/0.2 M NBu_4PF_6.

voltammograms before and after coulometry (Figure S34 in the Supporting Information) were nearly identical in terms of peak potentials, intensities, and the overall line shapes, thus indicating that the redox process is reversible on the voltammetry and the coulometry timescale.

Samples for EPR spectroscopy were taken after approximately 50% reduction (Figure 4) and after 99% reduction and were immediately frozen in liquid dinitrogen. A characteristic low g_3 value, as detected for the reduced $[2Fe\text{-}2S]^+$ cluster in Rieske proteins[12] ($g_3\approx1.78$–1.81) was observed for the 50% reduced sample by fitting the experimental EPR data with $g_1=2.014$, $g_2=1.936$, and $g_3=1.804$; g_1 is slightly lower and g_2 somewhat higher than the corresponding values found for Rieske proteins ($g_1\approx2.02$–2.03, $g_2\approx1.89$–1.90).[3a,13]

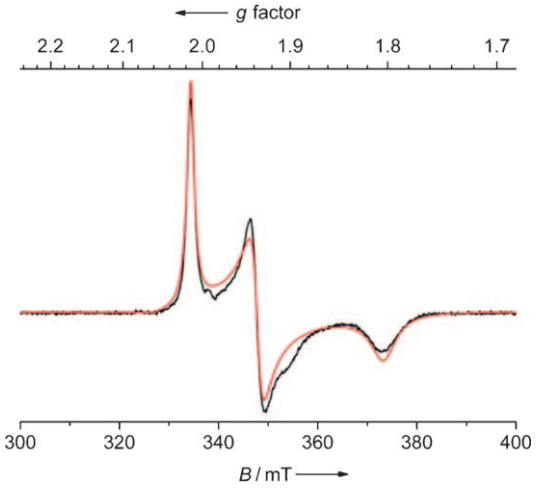

Figure 4. EPR spectrum of one-electron-reduced **4** (generated by constant-potential coulometry at −25 °C, −1.9 V vs. $[Cp_2Fe]/[Cp_2Fe]^+$, sample taken after ca. 50% reduction), recorded at 20 K in frozen MeCN/0.2 M NBu_4PF_6 ($c=3.94\times10^{-4}$ M, spectrometer frequency: 9.43198 GHz, microwave power 25 μW, modulation amplitude: 1 mT). ——: simulation of the experimental values (——) with $g_1=2.014$, $g_2=1.936$, and $g_3=1.804$.

The low averaged $g_{av} = 1.920$ for **4** (cf. $g_{av} = 1.90$–1.91 for Rieske proteins[3a,13] and $g_{av} = 1.95$–1.97 for ferredoxins;[14] Tables S3 and S4 in the Supporting Information) and the wide anisotropy of the main components of the g tensor (mainly a result of the low g_3 value) suggest that reduction takes place at the N-ligated iron atom of **4**. This lowering of g_3 and g_{av} in Rieske type [2Fe-2S]$^+$ species was previously attributed to a more pronounced orthorhombic C_{2v} distortion at the $\{N_2S_2\}$-surrounded tetrahedral ferrous ions.[15]

An improved agreement of the experimental values with the fit curve is observed for the 99% reduced sample, with virtually identical g values measured for the target material ($g_1 = 2.015$, $g_2 = 1.936$, $g_3 = 1.803$). However, a second, as yet unknown species (ca. 12%, delocalized $S = 1/2$ radical, fitted with $g_1 = 2.096$, $g_2 = 2.021$, and $g_3 = 1.906$) formed during the 100% CPC, probably owing to some over-reduction (Figure S37). The reduced [2Fe-2S]$^+$ species seems to be slightly unstable, also indicated by an increasing UV/Vis absorption after completed coulometry (measured 3.5 min after 100% CPC, no electrical current applied to the sample, but kept under argon at −25 °C; Figure S36 in the Supporting Information).

To corroborate conclusions from the EPR findings, DFT calculations were carried out with the Turbomole 5.9 software package[16a] using the Becke–Perdew-1986 functional (BP86)[16b,c] and the def2-SVP[16d] basis set. Both the oxidized and reduced forms of **4** were studied in the antiferromagnetically coupled spin state. Analysis of the molecular orbitals revealed a localization of the lowest unoccupied molecular orbital (LUMO) in oxidized **4** (Figure S40 in the Supporting Information) at the N-coordinate Fe atom. Accordingly, the highest occupied molecular orbital (HOMO) in reduced **4** (Figure 5) is located at this unique iron center, as previously concluded from DFT calculations on a fictitious mixed-valent Rieske type model system.[16e]

In conclusion, the first synthetic model for [2Fe-2S] Rieske sites reported herein adequately emulates structural, Mössbauer, and EPR parameters of the analogous protein-bound clusters. Future efforts will focus on the incorporation of additional nitrogen atoms into the $\{N_2\}$ ligand backbone to provide potential protonation sites that would allow the model to more closely mimic the electrochemical properties of the natural enzymes and to support the role of the iron-ligated histidines in the pH-dependence of the reduction potential.[11]

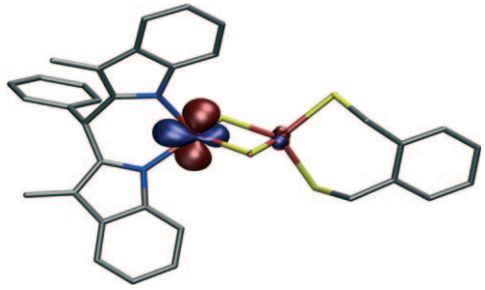

Figure 5. Illustration of the highest occupied molecular orbital (HOMO, contour value = 0.06) of **4** in the one-electron-reduced mixed-valent state; C gray, Fe red, N blue, S yellow. Hydrogen atoms are omitted for clarity.

Received: July 15, 2008
Published online: October 29, 2008

Keywords: bioinorganic chemistry · iron · Mössbauer spectroscopy · Rieske centers · sulfur

[1] a) J. S. Rieske, D. H. MacLennan, R. Coleman, *Biochem. Biophys. Res. Commun.* **1964**, *15*, 338–344; b) J. S. Rieske, *J. Biol. Chem.* **1968**, *239*, 3017–3022.
[2] a) T. A. Link, M. Saynovits, C. Assmann, S. Iwata, T. Ohnishi, G. von Jagow, *Eur. J. Biochem.* **1996**, *237*, 71–75; b) S. Iwata, M. Saynovits, T. A. Link, H. Michel, *Structure* **1996**, *4*, 567–579; c) H. Bönisch, C. L. Schmidt, G. Schäfer, R. Ladenstein, *J. Mol. Biol.* **2002**, *319*, 791–805; d) T. A. Link, O. M. Hatzfeld, M. Saynovits in *Bioinorganic Chemistry* (Ed.: A. X. Trautwein), Wiley-VCH, Weinheim, **1997**, pp. 312–325.
[3] a) J. A. Fee, K. L. Findling, T. Yoshida, R. Hille, G. E. Tarr, D. O. Hearshen, W. R. Dunham, E. P. Day, T. A. Kent, E. Münck, *J. Biol. Chem.* **1984**, *259*, 124–133; b) D. J. Ferraro, L. Gakhar, S. Ramaswamy, *Biochem. Biophys. Res. Commun.* **2005**, *338*, 175–190.
[4] P. V. Rao, R. H. Holm, *Chem. Rev.* **2004**, *104*, 527–559.
[5] a) D. Coucouvanis, A. Salifoglou, M. G. Kanatzidis, A. Simopoulos, V. Papaefthymiou, *J. Am. Chem. Soc.* **1984**, *106*, 6081–6082; b) J. Ballmann, X. Sun, S. Dechert, E. Bill, F. Meyer, *J. Inorg. Biochem.* **2007**, *101*, 305–312.
[6] A few symmetrical [2Fe–2S] clusters with mixed {NS} ligand sets at each iron have been reported: a) P. Beardwood, J. F. Gibson, *J. Chem. Soc. Dalton Trans.* **1992**, 2457–2466; b) Y. Ohki, Y. Sunada, K. Tatsumi, *Chem. Lett.* **2005**, *34*, 172–173.
[7] a) M. A. Bobrik, K. O. Hodgson, R. H. Holm, *Inorg. Chem.* **1977**, *16*, 1851–1858; b) Y. Do, E. D. Simhon, R. H. Holm, *Inorg. Chem.* **1983**, *22*, 3809–3812; c) G. B. Wong, M. A. Bobrik, R. H. Holm, *Inorg. Chem.* **1978**, *17*, 578–584.
[8] K. Dittmann, U. Pindur, *Arch. Pharm.* **1985**, *318*, 340–350.
[9] a) J. J. Mayerle, S. E. Denmark, B. V. DePamphilis, J. A. Ibers, R. H. Holm, *J. Am. Chem. Soc.* **1975**, *97*, 1032–1045; b) W. O. Gillum, R. B. Frankel, S. Foner, R. H. Holm, *Inorg. Chem.* **1976**, *15*, 1095–1100.
[10] a) J. A. Fee, K. L. Findling, T. Yoshida, R. Hille, G. E. Tarr, D. O. Hearshen, W. Dunham, E. P. Day, T. A. Kent, E. Münck, *J. Biol. Chem.* **1984**, *259*, 124–133; b) D. Kuila, J. A. Fee, *J. Biol. Chem.* **1986**, *261*, 2768–2771; c) P. J. Geary, D. P. E. Dickson, *Biochem. J.* **1981**, *195*, 199–203.
[11] a) D. J. Kolling, J. S. Brunzelle, S Lhee, A. R. Crofts, S. K. Nair, *Structure* **2007**, *15*, 29–38; b) T. Iwasaki, A. Kounosu, D. R. J. Kolling, A. R. Crofts, S. A. Dikanov, A. Jin, T. Imai, A. Urushiyama, *J. Am. Chem. Soc.* **2004**, *126*, 4788–4789; c) N. J. Cosper, D. M. Eby, A. Kounosu, N. Kurosawa, E. L. Neidle, D. M. Kurtz, Jr., T. Iwasaki, R. A. Scott, *Protein Sci.* **2002**, *11*, 2969–2973; d) Y. Zu, M. M.-J. Couture, D. R. J. Kolling, A. R. Crofts, L. D. Eltis, J. A. Fee, J. Hirst, *Biochemistry* **2003**, *42*, 12400–12408; e) A. R. Klingen, G. M. Ullmann, *Biochemistry* **2004**, *43*, 12383–12389; f) E. J. Leggate, J. Hirst, *Biochemistry* **2005**, *44*, 7048–7058; g) I-J. Lin, Y. Chen, J. A. Fee, J. Song, W. M. Westler, J. L. Markley, *J. Am. Chem. Soc.* **2006**, *128*, 10672–10673.
[12] a) M. Rampp, E. Kellner, A. Müller, A. Riedel in *Bioinorganic Chemistry* (Ed.: A. X. Trautwein), Wiley-VCH, Weinheim, **1997**, pp. 295–301; b) M. K. Bowman, E. A. Berry, A. G. Roberts, D. M. Kramer, *Biochemistry* **2004**, *43*, 430–436.

[13] a) J. N. Siedow, S. Power, F. F. De La Rosa, G. Palmer, *J. Biol. Chem.* **1978**, *263*, 2392 – 2399; b) S. De Vries, S. P. J. Albracht, F. J. Leeuwerik, *Biochim. Biophys. Acta Bioenerg.* **1979**, *546*, 316 – 333; c) R. C. Prince, *Biochim. Biophys. Acta Bioenerg.* **1983**, *723*, 133 – 138; d) R. Malkin, A. J. Bearden, *Biochim. Biophys. Acta Rev. Bioenerg.* **1978**, *505*, 147 – 181; e) B. L. Trumpower, C. A. Edwards, T. Ohnishi, *J. Biol. Chem.* **1980**, *255*, 209 – 223; f) F. Tiago de Oliveira, E. L. Bominaar, J. Hurst, J. A. Fee, E. Münck, *J. Am. Chem. Soc.* **2004**, *126*, 5338 – 5339.

[14] a) J. Fritz, R. Anderson, J. Fee, G. Palmer, R. H. Sands, J. C. M. Tsibris, I. C. Gunsalus, W. H. Orme-Johnson, H. Beinert, *Biochim. Biophys. Acta Bioenerg.* **1971**, *253*, 110 – 133; b) D. V. Devartanian, Y. I. Shethna, H. Beinert, *Biochim. Biophys. Acta Protein Struct.* **1969**, *194*, 548 – 563; c) J. A. Fee, G. Palmer, *Biochim. Biophys. Acta Bioenerg.* **1971**, *245*, 175 – 195; d) K. Mukai, T. Kimura, J. Helbert, L. Kevan, *Biochim. Biophys. Acta Protein Struct* **1973**, *295*, 49 – 56; e) P. Bertrand, J. P. Gayda, *Biochim. Biophys. Acta Protein Struct.* **1979**, *579*, 107 – 121.

[15] P. Bertrand, B. Guigliarelli, J.-P. Gayda, P. Beardwood, J. F. Gibson, *Biochim. Biophys. Acta Protein Struct. Mol. Enzymol.* **1985**, *831*, 261 – 266.

[16] a) R. Ahlrichs, M. Bär, M. Häser, H. Horn, C. Kölmel, *Chem. Phys. Lett.* **1989**, *162*, 165 – 169; b) A. D. Becke, *Phys. Rev. A* **1988**, *38*, 3098 – 3100; c) J. P. Perdew, *Phys. Rev. B* **1986**, *33*, 8822 – 8824; d) F. Weigend, R. Ahlrichs, *Phys. Chem. Chem. Phys.* **2005**, *7*, 3297 – 3305; e) M. Shoji, K. Koizumi, Y. Kitagawa, S. Yamanaka, M. Okumura, K. Yamaguchi, *Int. J. Quantum Chem.* **2007**, *107*, 609 – 627.

